Table I. Chemical Compositions and Lattice Constants of Mechanically Alloyed Cu-29.7 At. Pct Zn + C Powders

Mixed Compositions (At. Pct)	Chemical Analysis Carbon Compositions (At. Pct C)	Mechanically Alloyed Alloy Compositions (At. Pct)	Lattice Constant (nm)
Cu-29.7Zn + 10C	9.5	Cu-26.9Zn-9.5C	0.36746
Cu-29.7Zn + 20C	18.5	Cu-24.2Zn-18.5C	0.36749
Cu-29.7Zn + 30C	28.5	Cu-21.2Zn-28.5C	0.36759
Cu-29.7Zn + 40C	38.5	Cu-18.3Zn-38.5C	0.37654
Cu-29.7Zn + 50C	48.5*	Cu-18.3Zn-38.5C	0.37654

*Not washed in ethanol.

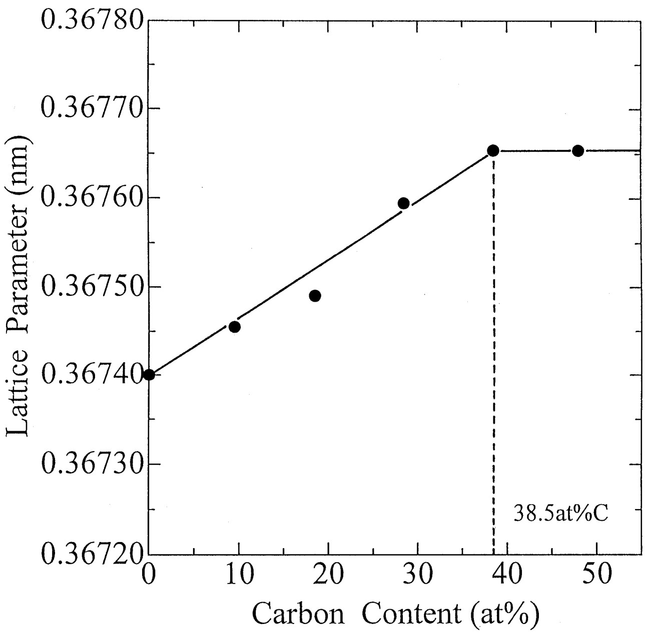

Fig. 3—Relation between lattice parameter of Cu-29.7 at. pct Zn alloy and solid solution concentration of carbon in α Cu-Zn phase.

lower angle side with increased milling time. The peak shifts correspond to the increase in the lattice parameter of the Cu-Zn alloy.

Figure 2 shows the changes in Cu-Zn alloy lattice parameters as a function of milling time. In all mixture powders, the lattice parameters increase and reach saturation values. Figure 3 indicates the relation between the lattice parameter and carbon content in solid solution in the Cu-Zn alloy. From the figure, the maximum supersaturated carbon concentration in solid solution in the Cu-Zn alloy is determined to be 38.5 at. pct C. Table I shows the chemical compositions and lattice constants of mechanically alloyed Cu-29.7 at. pct Zn + C powders. Saji *et al.*[6] reported previously that the maximum supersaturated carbon concentration in mechanically alloyed copper was 28.5 at. pct C. Comparing with copper, the maximum supersaturated solid solubility of carbon in the Cu-29.7 at. pct Zn alloy is higher.

REFERENCES

1. S. Abe, S. Saji, and S. Hori: *J. Jpn. Inst. Met.*, 1990, vol. 54, pp. 895-02.
2. K. Uenishi, K.E. Kobayashi, S. Nasu, H. Hanano, K.N. Ishihara, and P.H. Shingu: *Z. Metallkd.*, 1992, vol. 83, pp. 132-35.
3. S. Saji, H. Araki, K. Hashimoto, and E. Murata: *Mater. Trans. JIM*, 1996, vol. 37, pp. 1061-66.
4. H. Araki, S. Saji, T. Okabe, Y. Minamino, T. Yamane, and Y. Miyamoto: *Mater. Trans. JIM*, 1997, vol. 38, pp. 247-54.
5. U. Mizutami, T. Takeuchi, and T. Fukunaga: *Mater. Trans. JIM*, 1993, vol. 34, pp. 102-08.
6. A.Y. Yermakov, Y.Y. Yurchikov, and V.A. Barinov: *Phys. Metall. Metallogr.*, 1981, vol. 52 (6), pp. 50-58; *Fiz. Metall. Metalloved.*, 1981, vol. 52, pp. 1184-93.
7. S. Saji, T. Kadokura, H. Anada, and K. Notoya: *Mater. Trans. JIM*, 1998, vol. 39, pp. 778-81.
8. R.B. McLellen: *Scripta Metall.*, 1969, vol. 3, pp. 389-91.
9. *Binary Alloy Phase Diagrams*, T.B. Massalski, ed., ASM INTERNATIONAL, Materials Park, OH, 1990, vol. 1, pp. 839-40.
10. *Binary Alloy Phase Diagrams*, T.B. Massalski, ed., ASM INTERNATIONAL, Materials Park, OH, 1990, vol. 1, p. 899.

Secondary Hardening and Impact Fracture Behavior in Isothermally Aged Mo, W, and Mo-W Steels

K.B. LEE, H.R. YANG, and H. KWON

Secondary hardening steels in which the ultrahigh strength can be obtained by a fine dispersion of M_2C-type carbides have attracted significant attention for high-performance applications. The alloying elements Mo and W form the carbides of M_2C type, accompanying the dissolution of cementite of M_3C type during tempering (aging) in the range of 500 °C to 650 °C.[1,2,3] Since Mo forms M_2C carbides at lower temperatures where a relatively high dislocation density is sustained, an effectively fine dispersion of M_2C carbides can be accomplished, as compared to W, which forms M_2C carbides at higher temperatures, where the dislocation recovery is well advanced because of its slower diffusion.[1,2,3] Hence, a weak hardening occurs in the W steel compared with a strong hardening in the Mo steel. In contrast, the MoW steel exhibited both moderately strong hardening and considerable resistance to overaging.

After tempering in the secondary hardening range, however, embrittlement can occur. This embrittlement is referred to as secondary hardening embrittlement (SHE). Secondary hardening embrittlement can be classified into two types:

K.B. LEE, Contract Professor, and H. KWON, Professor, are with the School of Metallurgical and Materials Engineering, Kookmin University, Seoul 136-702, Korea; H. KWON is also with the Center for Advanced Aerospace Materials, POSTECH, Pohang 790-784, Korea. H.R. YANG, Professor, is with the Department of Mechanical Engineering, Inchun Junior College, Inchun 402-750, Korea.

Manuscript submitted February 28, 2000.

Table I. Chemical Composition of Experimental Alloys (Weight Percent)

Alloy Designation	C	Mo	W	P	S
MO steel	0.20	4.25	—		
W steel	0.25	—	5.47	0.005	0.005
MoW steel	0.25	2.13	2.83		

intergranular and transgranular SHE, according to the fracture mode. It has been suggested that the intergranular SHE is caused by impurity segregation resulting in easy intergranular fracture[4] and that transgranular SHE is associated with coarse boundary carbides leading to easy transgranular cleavage fracture.[5] In recent years, Kwon and co-workers[6–9] studied SHE in 1-hour isochronally aged Mo, W, and Mo-W steels. The intergranular SHE in an overaged condition occurred as compared to the transgranular SHE in the underaged condition for the Mo and Mo-W steels. In the W steel, however, SHE in an overaged condition occurred in a transgranular manner through the reduction in the upper shelf energy. Hence, the fracture behavior in SHE can be greatly affected by aging condition. However, since the relative aging condition merely can be indicated by the 1-hour isochronal aging, isothermal aging is required to find the real peak-aged condition.

The purpose of this study was to analyze secondary hardening and fracture behavior of Mo, W, and Mo-W steels containing basic M_2C carbide forming elements by means of isothermal aging.

Chemical compositions of experimental alloys are presented in Table I. Impact specimens were austenitized at 1200 °C for 1 hour under argon atmosphere and then water quenched. Aging (tempering) was isothermally performed at 600 °C. Details of the experimental procedure were presented in a previous article.[9]

Figure 1 shows the hardness variations with aging time at 600 °C. In the as-quenched condition, the hardness of the Mo steel was lower than the W and Mo-W steels because of the lower carbon content. However, the peak hardness of the Mo steel was, similarly to the Mo-W steel, higher as compared to the W steel. The time to peak hardness was 1 hour in the Mo steel, while it was 5 hours in the W and Mo-W steels. For the 1 hour isochronal aging at 550 °C, 600 °C, and 650 °C, the peak hardness was investigated at 600 °C in all steels.[9] Compared with the isothermal aging at 600 °C, however, while the 600 °C–1 hour is the real peak-aged condition in the Mo steel, it is not the real peak-aged but is the underaged condition in the W and Mo-W steels. In contrast, the hardness values of the 1-hour isochronal overaged condition (650 °C)[9] correspond to those of the 10- to 20-hour isothermal overaged condition at 600 °C.

The peak hardness to as-quenched hardness ratio was 45.8/41.4 (1.11), 46.7/45.5 (1.03), and 38.6/45.5 (0.85) in the Mo, Mo-W, and W steels, respectively. In the Mo steel, the secondary hardening was most effective in terms of both time and hardness, although the overaging was rapidly proceeded. However, the W steel showed a large resistance to overaging, while it presented a weak hardening at 5 hours and a significantly lower peak hardness to as-quenched hardness ratio. In the Mo-W steel, on the other hand, the moderately strong hardening was attributable to the effect of the

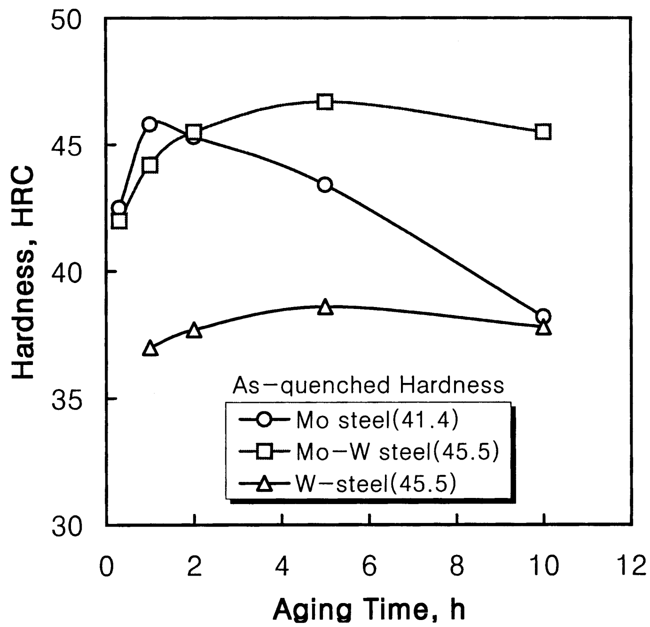

Fig. 1—Hardness variations with aging time at 600 °C in the Mo, Mo-W, and W steels.

Mo addition, while the peak aging occurred at a relatively long time of 5 hours due to the addition of W. These differences in aging behavior are associated with the precipitation of the M_2C carbide accompanying the dissolution of cementite, which is influenced by the alloying additions.

Figure 2 shows TEM micrographs in the peak-aged conditions. The needle- or rod-shaped M_2C carbides are arrayed into the ⟨100⟩ cube directions, while the platelike M_3C cementite has the {110} habit planes of the ferrite matrix. Hence, in the cube-oriented beam used in this study, M_2C carbides can be observed in two perpendicular ⟨100⟩ directions, while the M_3C cementite can be observed in two perpendicular ⟨110⟩ directions rotated by 45 deg with respect to the ⟨100⟩ directions.

In the peak-aged condition, while the Mo steel exhibited a high density of very fine M_2C carbides, the MoW represented a medium density of fine M_2C carbides. In the W steel, however, coarse cementite was still observed even in the peak-aged condition, as well as a low density of fine M_2C carbides. These microstructural differences in the peak-aged condition reflect well the strong, intermediate, and weak effect on the secondary hardening in the Mo, Mo-W, and W steels, respectively. In the Mo steel, the dense precipitation of very fine M_2C carbides following the cementite dissolution was achieved already in the 1-hour peak-aged condition. In the W steel, however, the formation of M_2C carbides was delayed due to the slow diffusion of W, and significant amounts of coarse cementite were retained even in the 5-hour peak-aged condition. In the Mo-W steel combined with Mo, on the other hand, the cementite, which had been observed in the 1-hour underaged condition, disappeared in the 5-hour peak-aged condition. Hence, the Mo-W steel exhibited the dual characteristics of the Mo and W additions.

Since the hardness of the 1-hour isochronal overaged condition (650 °C) corresponds to that of the 10- to 20-hour isothermal overaged condition at 600 °C, the transmission

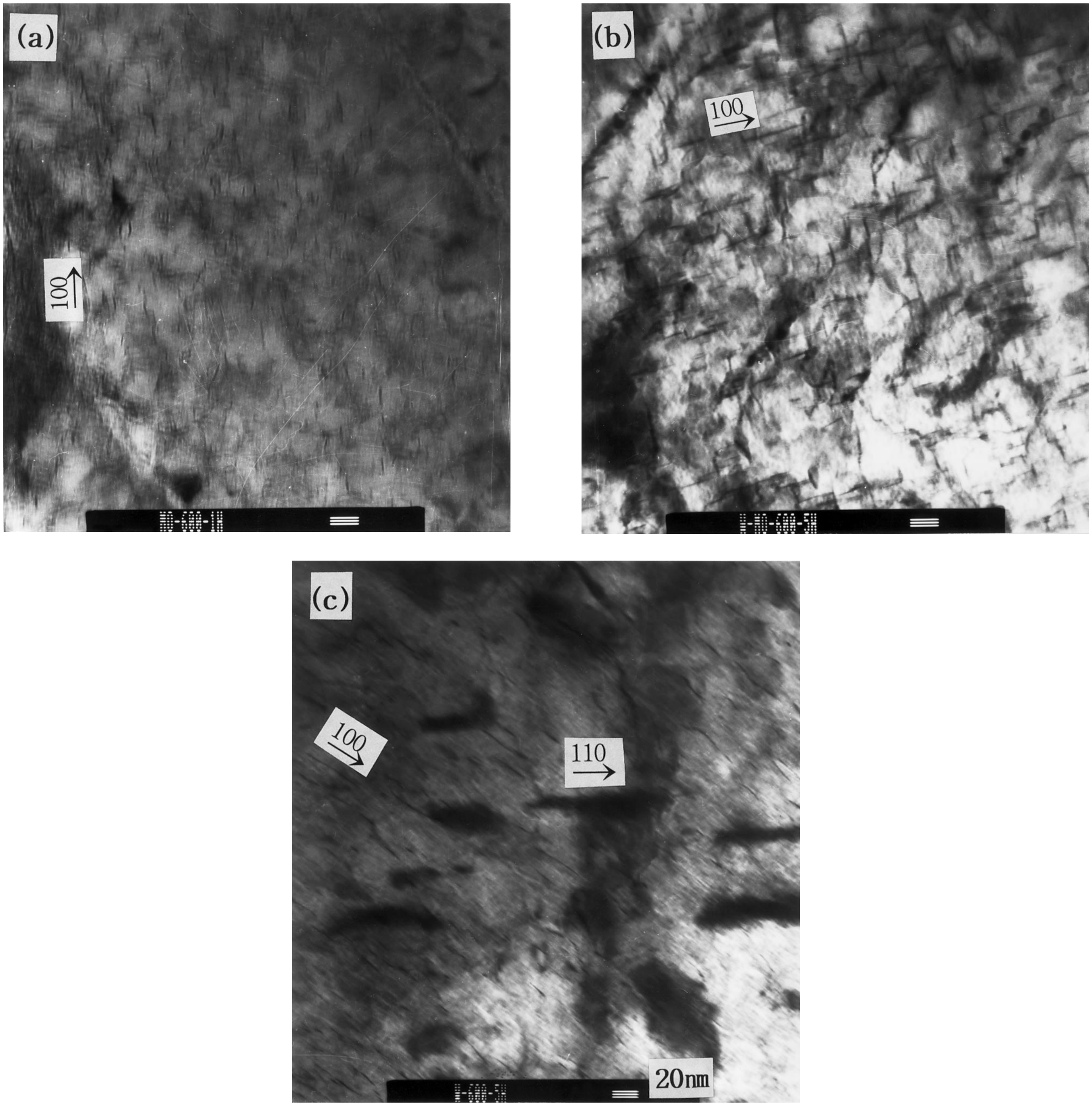

Fig. 2—TEM micrographs observed in the cube oriented beam for the peak-aged specimens: (*a*) 1 h aging in the Mo steel, (*b*) 5 h aging in the Mo-W steel, and (*c*) 5 h aging in the W steel.

electron micrographs in Reference 9 are referred. On overaging in the Mo and MoW steel, the M_2C carbides grew rapidly and slowly after almost complete dissolution of cementite, as shown in Figures 4 and 5 in Reference 9, respectively. In the W steel, however, not only the relatively fine M_2C carbides, whose distribution was not dense, but the coarse cementite were also present even in the overaged condition, as shown in Figure 6 in Reference 9. In other words, it is not possible to achieve an effective hardening that could be produced by the dense precipitation of fine M_2C carbides accompanied with the almost complete dissolution of cementite in the W steel. Hence, in the W steel, the M_2C carbides to be formed in the much recovered dislocation network for the longer time overaged condition could not be densely dispersed. Their growth thus resulted in a continuous decrease in hardness, although the overaging slowly went on due to the slow diffusion of W. In the Mo-W steel, the slow overaging was also caused by the W addition.

In the previous studies[6–9] on the same steels isochronally aged, the fracture occurred in a transgranular manner in the underaged condition in all steels. On the other hand, significant amounts of the intergranular fracture were investigated in the Mo and Mo-W steels, but the intergranular fracture was not investigated in the W steel, particularly in the overaged condition. Since the same fracture behavior was also observed on the same steels isothermally aged, the fracture surfaces are similar to those presented in References 8 and 9.

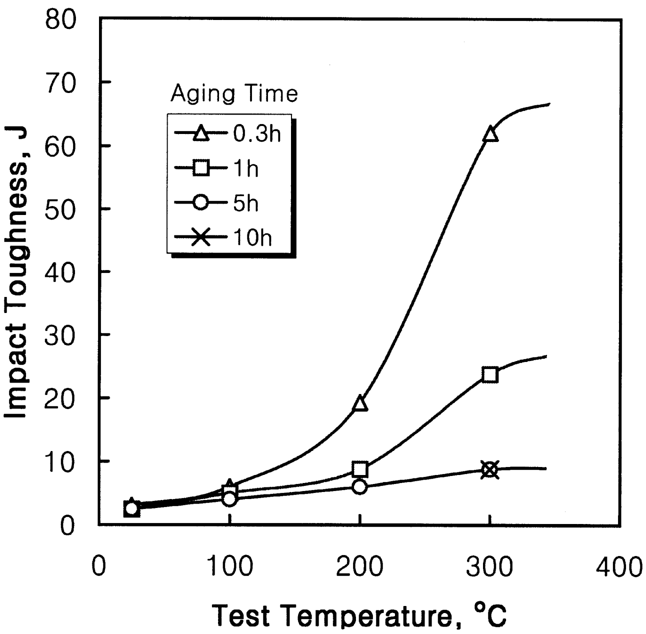

Fig. 3—Variations in impact toughness with test temperature for the Mo steel.

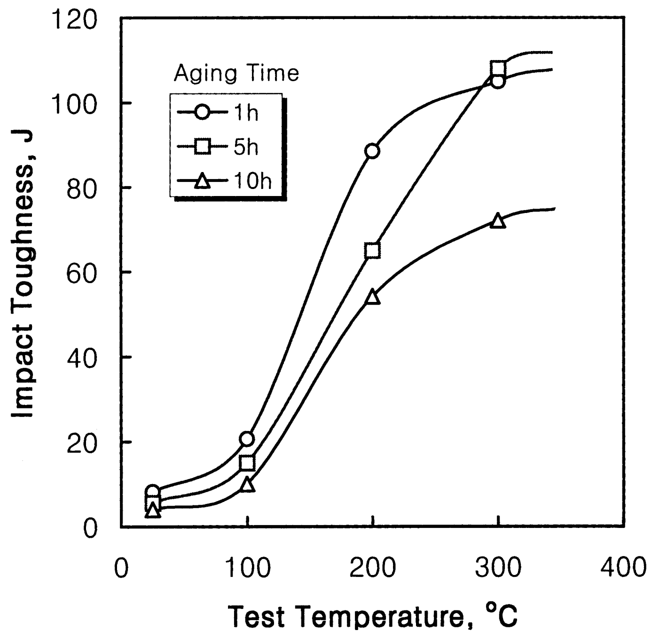

Fig. 5—Variations in impact toughness with test temperature for the W steel.

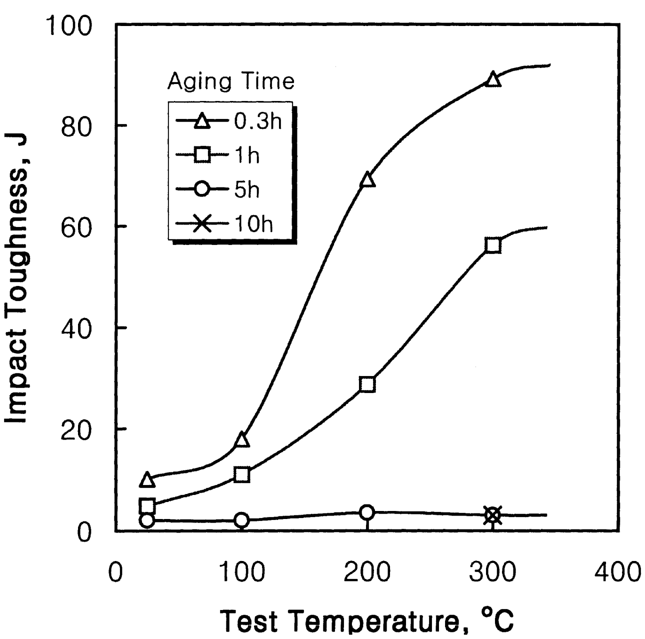

Fig. 4—Variations in impact toughness with test temperature for the Mo-W steel.

Figure 3 shows the variations in impact toughness with test temperature for the Mo steel. While in the underaged condition (0.3 hours), the impact toughness was recovered to the upper shelf energy of 65J at 300 °C, its recovery was small (25 J) and very small (9 J) in the peak-aged (1 hour) and overaged (5 hour) conditions, respectively. In the isochronally peak-aged and overaged conditions, the SHE was attributed to the occurrence of intergranular fracture, associated with the impurity (P) segregation at the grain boundaries. The segregation of P on the intergranular fracture surfaces in the overaged condition (650 °C–1 hour) was identified by Auger electron spectroscopy (AES) analysis in a previous article.[9] The P peak (120 eV), whose height is about 0.04 relative to the height of the Fe peak (703 eV), is clearly detected on the intergranular area, but not on the transgranular area.

Figure 4 shows the variations in impact toughness with test temperature for the Mo-W steel. In the underaged conditions (0.3 and 1 hours), the upper shelf energy decreased from 89 to 56 J with an increase in aging time. In the peak-aged (5 hours) condition, however, the impact toughness was not recovered with an increase in test temperature and remained at a very low level of 3 J even at 300 °C. In the overaged condition (10 hours), the same behavior was observed. Secondary hardening embrittlement in the peak-aged and overaged conditions also resulted from the occurrence of intergranular fracture. This embrittlement also may be caused by the impurity segregation at the grain boundaries, even though no direct AES analysis was conducted.

Intergranular fracture can be caused by impurities and/or carbides at the grain boundaries. The impurities directly affect the grain boundary strength, while the carbides act as stress concentrators (*i.e.*, slip barriers). It was suggested that the Mo and W in the matrix could tie up P, presumably by lowering its activity or by the formation of Mo(W)-phosphides for the underaged condition.[9,10,11] For the overaged condition, however, the released P, due to the depletion of Mo(W) in matrix after the almost complete precipitation of M_2C carbides, could segregate to the grain boundaries. In the Mo steel overaged at 650 °C for 1 hour, the P was clearly detected on the intergranular area, while it was not detected on the transgranular one. In addition, there were the coarse Mo-carbides at the lath boundaries.[9] Hence, the combined action of impurities and relatively coarse Mo(W)-carbides at the grain boundaries seems to produce the intergranular embrittlement even though the hardness is decreased in the overaged condition.

Figure 5 shows the variations in impact toughness with test temperature for the W steel. The upper shelf energy was lowered from 110 J in the peak-aged condition (5 hours) to 70 J in the overaged condition (10 hours). Since the fracture occurred in a mostly transgranular manner,[8,9] the embrittlement was not severe, as compared to the intergranular embrittlement, which produced very low impact toughness values below 10 and 5 J, even at 300 °C, in the Mo and MoW steels, respectively. In the overaged condition, since the presence of cementite[9] indicates that there are sufficient amounts of W available to tie up the P, no severe intergranular embrittlement could occur.

This work was partly supported by the POSCO.

REFERENCES

1. J.J. Irani and R.W.K. Honeycomb: *J. Iron Steel Inst.*, 1966, vol. 203, pp. 826-33.
2. D. Raynor, J.A. Whiteman, and R.W.K. Honeycomb: *J. Iron Steel Inst.*, 1966, vol. 204, pp. 349-54.
3. A.T. Davenport and R.W.K. Honeycomb: *Met. Sci.*, 1975, vol. 9, pp. 201-08.
4. M.K. Tseng, D.Y. Lee, and H.L. Marcus: *Mater. Eng. Sci.*, 1983, vol. 60, pp. 73-77.
5. H. Kwon and C.H. Kim: *Metall. Trans. A*, 1983, vol. 14A, pp. 1389-94.
6. H. Kwon: *Scripta Metall.*, 1989, vol. 23, pp. 1001-04.
7. H. Kwon: *Metall. Trans. A*, 1991, vol. 22A, pp. 1119-22.
8. K.B. Lee and H. Kwon: *Scripta Metall. Mater.*, 1992, vol. 24, pp. 1355-60.
9. H. Kwon, K.B. Lee, H.R. Yang, J.B. Lee, and Y.S. Kim: *Metall. Mater. Trans. A*, 1997, vol 28A, pp. 775-84.
10. C.J. McMahon, Jr., A.K. Cianelli, and H.C. Feng: *Metall. Trans. A*, 1977, vol. 8A, pp. 1055-57.
11. J.I. Ustinovshchikov: *Acta Metall.*, 1983, vol. 31, pp. 355-64.

Mean Strain Effects on the Fatigue Properties of Superelastic NiTi

R.M. TABANLI, N.K. SIMHA, and B.T. BERG

NiTi belongs to a class of materials called superelastic materials or shape-memory alloys. These alloys perform the largest amount of work per unit mass and per cycle and are capable of recovering strains as large as 6 pct in a reversible manner. Hence, they are ideal candidates for actuator and large-deformation biomedical applications. Predominantly, fatigue studies of superelastic materials[1,2,3] have obtained stress amplitude *vs* cycles-to-failure (S–N) curves and crack growth rates under completely reversed cyclic loading. However, as Miyazaki[4] argues, completely reversed loading is irrelevant to the superelastic working cycle. Hence, Miyazaki has measured S–N curves for loads that cycled between zero and a maximum stress.[4] The deformation corresponding to the low- and high-cycle fatigue was different; stress-induced transformation was observed in low-cycle fatigue, but not in high-cycle fatigue. This difference is also reflected in the S–N curves, where lines with different slopes are needed to fit the high-cycle and low-cycle data.

The martensitic transformation is the basis of the superelastic and shape-memory properties. Yet, most existing studies do not explore the influence of the martensitic transformation on fatigue properties. The study by Miyazaki[4] shows that the martensitic transformation can influence the fatigue properties, but does not explicitly examine it. We propose to examine the influence of the martensitic transformation on the fatigue properties of NiTi by exploring mean-strain effects on the fatigue properties. Mean stress and mean-strain determine the phase of the material in superelastic specimens. Depending on the mean strain, a specimen may contain austenite (A), martensite (M), or both phases (AM), and different deformation modes are associated with each of these cases. In numerous applications, loads cycle with a tensile mean strain, and, in particular, this research is relevant to cardiovascular stents.[5]

This article examines the effect of a mean cycling strain on the fatigue properties of superelastic NiTi. First, we propose a phase diagram in the space of mean strain and strain amplitude. This will aid in the systematic design of fatigue experiments that examine mean-strain effects. Second, we report results of tests on polycrystalline NiTi tubes that demonstrate mean-strain effects on cycles to failure.

A typical superelastic loading-unloading curve for NiTi is shown in Figure 1(a). The values of the various parameters are $\varepsilon_f = 0.8$ pct, $\varepsilon_f + \varepsilon_t = 6.4$ pct, and $\varepsilon_r = 6$ pct. Previous studies[6,7] have established the following. (1) During loading, the specimen contains B2-austenite in the strain range $0 < \varepsilon < \varepsilon_f$; at ε_f, the austenite becomes unstable, B19′-martensite forms in certain regions, and as the strain increases more and more material converts to M, until the entire specimen transforms at $\varepsilon_f + \varepsilon_t$; further straining results first in the detwinning and later in the elastic (and some plastic) deformation of the M. (2) During unloading, the M remains stable until the strain decreases to ε_r, when parts of the specimen transform back to A. More and more material converts back to A as the strain decreases, and at $\varepsilon_r - \varepsilon_t$, the entire specimen is in the A phase. We reiterate that the mechanism of deformation is different in the A, plateau, and M regions. The A deforms elastically. The deformation corresponding to the plateaus is due to the phase transformation: either due to nucleation of new regions or due to the interface-driven growth of existing regions. The M deformation is primarily due to detwinning with some contributions from elastic and plastic deformation.

Unloading from the upper plateau or loading from the lower plateau results initially in elastic deformation (Figure 1(b)). Subsequently, when the unloading reaches the lower plateau or the loading reaches the upper plateau, the volume fractions of the two phases change. During the elastic deformation in these smaller loops, the specimen resembles a composite material containing bimaterial interfaces separating A and M phases.

It follows from the preceding description that a small strain superimposed on a fixed strain can trigger either the forward or the reverse transformation depending on the value of the fixed strain. Hence, it is essential to map the regions where phase transformation occurs in the space of mean strains and strain amplitudes (ε_m, ε_a). From Figure 1, we

---

R.M. TABANLI, Assistant Professor, is with the Faculty of Mechanical Engineering, Istanbul Technical University. N.K. SIMHA, Assistant Professor, is with the Department of Mechanical Engineering, University of Miami, Coral Gables, FL 33124-0624. B.T. BERG, Research Scientist, is with Scimed Life Systems, Inc., Minneapolis, MN 55311-1566.

Manuscript submitted February 2, 2000.